Erosion of Natural Cooling Infrastructure in Southeast Asian Cities: Comparative Land Surface Temperature Effects of Wetland and Paddy Loss in Phnom Penh and Can Tho

Author name: Lik Ren, Tai
Affiliation: Woosong University, Daejeon, Korea
Email address: likrentai@gmail.com
ORCID: 0009-0002-6667-3331

Erosion of Natural Cooling Infrastructure in Southeast Asian Cities: Comparative Land Surface Temperature Effects of Wetland and Paddy Loss in Phnom Penh and Can Tho

Lik Ren Tai*

Woosong University, Daejeon, Korea (ORCID iD: 0009-0002-6667-3331)

Abstract

Rapid urbanisation across Southeast Asia is displacing two distinct forms of natural cooling infrastructure: urban water bodies and peri-urban paddy fields. The land surface temperature (LST) consequences of each have rarely been quantified using consistent, satellite-based methods, and have never been compared directly within a single study design. This study compares urban wetland loss in Phnom Penh, Cambodia, and paddy conversion in Can Tho, Vietnam, across six anchor epochs (2000–2024), using Landsat-derived land-cover classification and a difference-in-differences design to isolate conversion-attributable LST anomalies from background warming. In Phnom Penh, water-body loss produced a DiD-corrected anomaly of 7.13°C, concentrated in a small number of large, documented infilling events. In Can Tho, paddy loss produced a smaller anomaly of 0.55°C, diffused across thousands of small, independent conversions. The comparative synthesis does not resolve to a single answer: measured as per-unit-area intensity, Phnom Penh's loss is roughly seven times more severe; measured as total city-wide thermal impact, Can Tho's far larger converted extent gives it the greater aggregate impact instead. This asymmetry reflects a deeper structural contrast in how the two cities lose cooling infrastructure, Phnom Penh through concentrated, large-scale events and Can Tho through diffuse, many small conversions, with direct implications for how mitigation should be designed in each context. The findings show that the thermal cost of cooling-infrastructure loss cannot be captured by a single metric common to both resource types: it depends on which resource is lost, how much is lost, and whether severity or scale is the question being asked.

Keywords: Urban heat island; Land surface temperature; Wetland loss; Paddy field conversion; Southeast Asia; Remote sensing

Article highlights:

- Phnom Penh water loss drives a 7.13°C DiD-corrected LST anomaly
- Can Tho paddy loss drives a smaller, diffuse 0.55°C LST anomaly
- Phnom Penh's per-area cooling-loss intensity is ~7x Can Tho's
- Can Tho's total city-wide thermal impact is ~3x Phnom Penh's instead
- Reproducible open-data workflow transfers to other SEA secondary cities

---

1. Introduction

1.1 Motivation

Rapid urbanisation across Southeast Asia continues to erode the natural cooling infrastructure embedded in and around secondary cities. Two distinct processes illustrate this pressure: the wholesale elimination of urban lakes and wetlands, and the conversion of peri-urban paddy rice fields to built-up land. Both processes reduce the evapotranspirative and thermal-buffering capacity of the landscape, yet their consequences for land surface temperature (LST) have rarely been examined using consistent, satellite-based methods at the city scale, and have not previously been examined within a single comparative study design spanning both mechanisms. This study addresses that gap through a two-city comparison: urban wetland loss in Phnom Penh, Cambodia, and paddy cooling decline in Can Tho, Vietnam.

Both processes have been extensively documented in governance, land rights and agricultural economics literature, but have not previously been examined through the lens of land surface temperature change. Combining Landsat-derived land use and land cover (LULC) classification, land surface temperature retrieval, and a difference-in-differences analytical design, this study quantifies the thermal consequence of cooling-infrastructure loss in both cities across six anchor epochs spanning 2000 to 2024 (2000, 2005, 2010, 2015, 2020 and 2024), and compares the two mechanisms directly within a single, consistent methodological framework.

1.2 Research Gaps

Two independently confirmed research gaps frame this study.

Gap 1 (Can Tho): paddy rice fields provide a measurable evapotranspirative cooling effect. Recent global satellite mapping, using an 8-day, 500 m MODIS-derived phenological rice-mapping framework (GlobalRice500), has established that paddy fields reduce daytime land surface temperature by 0.21–0.27°C during the growing season relative to other croplands (Weng et al., 2026). This effect has, however, only been quantified at the global scale to date; its thermal consequence at the city scale, specifically the conversion of peri-urban paddy to built-up land in a rapidly urbanising Southeast Asian secondary city, has not previously been studied.

Gap 2 (Phnom Penh): Phnom Penh's urban lakes and wetlands have undergone extensive infilling since the early 2000s. Documentary evidence indicates that 16 of the city's 25 mapped urban lakes had been fully infilled by 2019, with the remainder partially filled, and that more than 40 percent of total wetland area had been lost over the same period (Sahmakum Teang Tnaut, 2019). No peer-reviewed study has yet quantified the land surface temperature consequence of this documented water body loss using satellite thermal data.

1.3 Research Questions and Hypotheses

Three research questions govern the study (Table 1). RQ1 and RQ2 are city-specific; RQ3 is the comparative synthesis question that justifies the two-city design.

Table 1. *Research questions addressed by this study.*

ID	Research Question
RQ1	In Phnom Penh, how has the systematic infilling of urban lakes and wetlands between 2000 and 2024 altered land surface temperature (LST) in formerly water-covered zones, and what is the magnitude of the cooling capacity that has been lost?
RQ2	In Can Tho, how has the conversion of peri-urban paddy fields to built-up land between 2000 and 2024 reduced the evapotranspiration-driven cooling function of agricultural land, and what LST increase is attributable to this conversion?
RQ3	Do the two cities exhibit systematically different LST outcomes from their respective cooling infrastructure losses, and what does this comparison reveal about which category of natural cooling resource, urban water bodies or peri-urban paddy agriculture, represents the higher thermal risk when removed?

Three working hypotheses accompany the research questions (Table 2), derived from published findings in comparable tropical urban contexts. Hypothesis direction and magnitude estimates are drawn from the literature reviewed in Section 1.2; actual values are reported and evaluated against these estimates in the Results and Discussion.

Table 2. *Working hypotheses, with estimated direction and magnitude drawn from comparable tropical urban contexts.*

ID	Hypothesis
H1	Locations of former lake and wetland surfaces in Phnom Penh will exhibit significantly higher LST (estimated +2 to +5°C) relative to periods before infilling, after controlling for seasonal variability.
H2	Peri-urban zones in Can Tho where paddy fields have been converted to built-up land will show a measurable LST increase (estimated +1.5 to +3°C) relative to unconverted paddy reference zones in the same climatic context.
H3	The per-unit-area thermal consequence of water body loss (Phnom Penh) will exceed that of paddy loss (Can Tho), reflecting the greater latent heat flux of open water relative to periodically flooded agricultural land.

1.4 Novel Contributions

This study makes four specific contributions to the literature. First, it provides the first satellite-based quantification of the land surface temperature consequences of urban lake and wetland elimination in Phnom Penh. Second, it provides the first city-scale application of the paddy evapotranspirative cooling framework of Weng et al. (2026) to a Southeast Asian secondary city. Third, it presents the first two-city comparative study contrasting the thermal consequences of two distinct categories of natural cooling infrastructure loss, open water elimination and paddy conversion, in secondary Southeast Asian cities. Fourth, it offers a methodological template, built entirely from freely available satellite datasets, that is applicable to any tropical secondary city experiencing loss of natural cooling infrastructure to urban expansion.

2. Study Area and Data

2.1 Study Sites and Administrative Boundaries

The study compares two Southeast Asian secondary cities: Phnom Penh, Cambodia, and Can Tho, Vietnam (Section 1). For each city, the study extent is defined as the city's administrative boundary plus a 10 km buffer, capturing peri-urban fringe dynamics beyond the formal city limit. All spatial analysis uses a common coordinate reference system, EPSG:32648 (UTM Zone 48N).

2.1.1 Phnom Penh

Phnom Penh's administrative boundary was constructed by dissolving admin2-level district polygons covering the city, downloaded during Phase 1 of this study. This file was recorded at the time of download as a GADM boundary; while preparing this section, however, its field structure (adm2_pcode, cod_versio, valid_on, valid_to) was found to match the UN Office for the Coordination of Humanitarian Affairs (OCHA) Common Operational Dataset – Administrative Boundaries (COD-AB) schema rather than GADM's (GID_n/NAME_n). The file is therefore an OCHA/ITOS COD-AB product (admin2, version V_01, valid_on 4 October 2018), not GADM, and is cited as such throughout this manuscript (Section 2.3).

Cambodia has not undergone an administrative merger comparable to Vietnam's (Section 2.1.2), so this mislabelling is a citation-provenance issue only: the underlying district geometry is unaffected, and no reanalysis of Phnom Penh data was required as a result of this correction. As a further check, the Phnom Penh boundary was compared against OpenStreetMap's current administrative boundary for the city, queried via *osmnx*. Total area differs by under 1% (688.50 km² for OSM against 684.24 km² for the reconstructed boundary used in this study), and a visual overlay shows the two boundaries closely aligned along the great majority of the perimeter, with only localised, sub-district-scale divergence in a small number of places. Given that Phnom Penh's constituent districts range from 2.2 to 148.4 km² in area, this pattern is consistent with ordinary boundary-digitisation differences between the two sources rather than the omission of a complete administrative district.

2.1.2 Can Tho

Can Tho's administrative boundary required substantive correction. The file used throughout Phases 2–4 of this study (vnm_admin1.shp) was, like Phnom Penh's, an OCHA/ITOS COD-AB product mislabelled as GADM; unlike Phnom Penh, this had a material geometric consequence, because it reflects Vietnam's 1 July 2025 provincial merger (63 provinces reduced to 34). The single 'Can Tho city' row in this file corresponds to the new, merged Can Tho–Hậu Giang–Sóc Trăng entity (6,360.82 km²), not the historical, pre-merger city (approximately 1,439 km²) around which the study was designed. Both the Landsat compositing and LULC classification pipelines filtered on this single row, so the merged-province geometry fed every Can Tho satellite export through Phase 4.

This was identified and corrected during manuscript preparation: a fresh, genuine GADM v4.1 boundary (GID_1='VNM.12_1') was downloaded, matching the historical city extent (1,438.65 km², buffered to 3,566.01 km²). All Can Tho rasters and derived statistics reported in this manuscript were re-clipped and recomputed against this corrected boundary; the diagnostic and correction workflow, and a module-by-module account of which results changed as a result, are described in the Methodology (Section 3.3 – 3.10). Phnom Penh required no equivalent rework.

2.1.3 Landsat WRS-2 Tiles

Both cities were verified to lie on Landsat World Reference System-2 (WRS-2) tiles Path 126/Row 52 (Phnom Penh) and Path 125/Row 53 (Can Tho). These were confirmed via Earth Engine scene-metadata checks (centroid stability across 2000, 2020 and 2024; a buffer-overlap test showing 97.6% of the Can Tho study area falling within a single tile) and cross-checked against the independent USGS EROS Earthshots archive for Phnom Penh, superseding an earlier, incorrect assumption (Path 124, Rows 054/055) in the original study design. The two cities sit on adjacent paths, imaged approximately one day apart within the same 16-day repeat cycle, supporting near-simultaneous comparative analysis under the same monsoon cloud cycle without implying literally identical acquisition dates.

2.1.4 Known Events

Phnom Penh's water-body loss includes several documented named events. Boeung Kak's infilling is dated to 2007–2011. Cheung Ek and Boeung Tompun are documented as having experienced ongoing losses over a broader, less precisely dated period. In the LST anomaly analysis (Section 3.5), Cheung Ek and Boeung Tompun are treated as a single, contiguous wetland complex, on documentary evidence that the two water bodies are connected rather than separable; Boeung Kak is treated as a distinct, separately dated event.

Can Tho's peri-urban expansion is documented as having proceeded along the Bassac River corridor since approximately 2005. The cluster-based analysis in Section 4.2.2 characterises the resulting conversion pattern as diffuse, distributed across many small, independent conversions rather than concentrated in a small number of large clusters; this is a finding about the size distribution of conversion events and does not speak to their spatial relationship to the river corridor specifically, which this study did not separately test (see Section 5.8, Future Work, for the deferred Bassac River distance-binning analysis).

2.2 Study Period and Satellite Sensors

The study spans six anchor epochs (2000, 2005, 2010, 2015, 2020 and 2024). For each epoch, dry-season composites were built from a 3-month window (primary: January–March; fallback: November–March, applied where primary-window valid-pixel coverage fell below 85%), following Collection 2 QA_PIXEL CFmask cloud and cloud-shadow masking. A parallel set of wet-season composites (May–October) was built for the seasonal-comparison sub-analysis (Method M9). These primary and fallback windows reflect the region's monsoon cloud-cover cycle, summarised in Table 3.

Table 3. *Monthly cloud-cover characterisation, both cities, motivating the dry-season compositing windows (Section 2.2).*

Month	Phnom Penh (Path 126/Row 052)	Can Tho (Path 125/Row 053)
Jan	Very good (15–25% heavy cloud)	Very good (15–25% heavy cloud)
Feb	Excellent (10–20%)	Excellent (10–20%)
Mar	Good (15–25%)	Good (15–25%)
Apr	Acceptable (25–35%)	Acceptable (25–35%)
May	Poor: monsoon onset (60–75%)	Poor: monsoon onset (60–75%)
Jun–Sep	Very poor (70–85%)	Very poor (70–85%)
Oct	Poor: late monsoon (50–65%)	Poor: late monsoon (50–65%)
Nov	Improving (25–35%)	Improving (25–35%)
Dec	Good (15–25%)	Good (15–25%)

Sensor coverage was confirmed directly from the acquisition notebooks rather than assumed from the original study design: Landsat 7 was planned in the original design but never queried in either the LST or surface-reflectance (SR) compositing pipelines, and does not appear in this study. Table 4 summarises which sensor generation contributed to each epoch.

Table 4. *Landsat sensor coverage by anchor epoch, both cities.*

Epoch	Sensor	Role
2000, 2005, 2010	Landsat 5 TM	LST and SR composites
2015, 2020	Landsat 8 OLI/TIRS	LST and SR composites
2024	Landsat 8 OLI/TIRS + Landsat 9 OLI-2/TIRS-2 (merged)	LST and SR composites

Band harmonisation between sensor generations is a deliberate methodological step: Landsat 5's band numbering differs from Landsat 8/9's (for example, the red band is SR_B3 on Landsat 5 but SR_B4 on Landsat 8/9). Bands were remapped to common names (blue, green, red, nir, swir1, swir2) before computing NDVI, NDWI and NDBI, ensuring spectral indices are computed consistently regardless of which sensor generation supplied a given epoch.

Valid-pixel coverage after cloud masking was 99–100% for Phnom Penh across all six epochs. Can Tho coverage ranged from 84.4% to 95.6%; the 2005 epoch fell just under the 85% primary-window threshold (84.4%) and used the November–March fallback window, reflecting a genuinely data-scarce acquisition year rather than a processing error. Both cities lie on adjacent WRS-2 paths (Section 2.1.3) and experience the same regional tropical monsoon cloud cycle, so the two columns in Table 3 are identical by the nature of the regional climatology rather than as a data-entry simplification.

2.3 Dataset Inventory

All datasets used in this study are freely accessible; no proprietary data, fieldwork or institutional data-sharing agreements were required. Table 5 summarises the primary datasets, their role in the analytical pipeline (Section 3), and their source citation.

Table 5. *Dataset inventory: resolution, role in the analytical pipeline, and source.*

Dataset	Resolution / cadence	Role	Source
Landsat 5 TM / 8 OLI-TIRS / 9 OLI-2-TIRS-2, Collection 2 Level-2	30 m / 16-day (8-day combined L8+L9)	Primary LST (Surface Temperature product) and SR source for LULC classification, both cities	U.S. Geological Survey
JRC Global Surface Water	30 m / annual	Annual water classification, Phnom Penh; change detection (M4, Tier 1)	Pekel et al. (2016)
GlobalRice500	500 m / annual (nearest-epoch matched: 2001, 2005, 2010, 2015, 2020, 2022)	Annual paddy-presence validation, Can Tho (M3)	Weng et al. (2026)
GHSL GHS-BUILT-S	100 m / 8 epochs, 1975–2020	Built-up validation for LULC classification, both cities (M2, M3)	Schiavina et al. (2023)
GHSL GHS-SMOD	1 km / 5 epochs, 2000–2020	Settlement-morphology classification (M10)	Schiavina et al. (2023)
SRTM Digital Elevation Model	30 m	Elevation, slope and aspect covariates for reference-zone matching (M6)	Farr et al. (2007)
Administrative boundary, Phnom Penh	Vector, admin2 (dissolved)	Study-area delineation	OCHA/ITOS (2018)
Administrative boundary, Can Tho	Vector, admin1 (GID_1='VNM.12_1')	Study-area delineation (corrected boundary, Section 2.1.2)	GADM (2022)
OpenStreetMap water bodies	Vector, current	Reference geometry for Phnom Penh's surviving water bodies (M5/M6, M8) and for the Bassac River corridor and general water context in Can Tho (Figure 2)	OpenStreetMap contributors (2026)
Google Earth Engine	Cloud platform	Acquisition, cloud masking, compositing, and extraction of all satellite datasets above	Gorelick et al. (2017)
Landsat WRS-2 Descending Path/Row grid	Vector, global scene grid	Tile-footprint delineation for Figure 2 (Path 126/Row 52, Phnom Penh; Path 125/Row 53, Can Tho)	U.S. Geological Survey
Natural Earth Admin 0 – Countries	1:50m vector	Regional country context for the Figure 1 locator map	Natural Earth

One item in Table 5 carries a methodological note, disclosed here for transparency. GHS-BUILT-S and GHS-SMOD are both drawn from the same JRC GHSL P2023A data package and share a single citation (Schiavina et al., 2023); neither dataset extends to 2024, so the nearest available prior epoch (2020) was used for periods requiring it, consistent with the nearest-epoch matching convention already applied to GlobalRice500. The OpenStreetMap water-body pull date, previously unresolved, was determined from the local file creation timestamp of the original acquisition (PhnomPenh_water.gpkg, created 29 June 2026), in the absence of a recoverable query log; this is a reasonable proxy given the file is the original download rather than a copy, but is disclosed as such rather than treated as an exact, logged access date.

The JRC Global Surface Water dataset's annual classification is provided under the band name waterClass; this corrects an earlier working assumption (yearly_classification) carried in preliminary planning documents, and is noted here since the two names could otherwise cause confusion when consulting the Earth Engine catalog entry directly. The three datasets with the longest temporal reach in this study do not share a common end year: Landsat-derived LST extends through 2024, GlobalRice500 through 2022, and JRC Global Surface Water through 2021. Cross-referencing between these datasets therefore relies on nearest-epoch matching, already noted above for GlobalRice500 and GHSL; this is disclosed here as a single, combined limitation on the temporal precision of any comparison spanning more than one of these three datasets, and is revisited in the Discussion (Section 5.7).

2.4 Study Area Figures

Two figures orient the reader to the study sites before the analytical results are presented. Both figures were constructed from the vector layers described above using Python (geopandas) for spatial data preparation and QGIS for cartographic styling, multi-panel layout and export (Section 3.11).

Figure 1. *Regional locator map showing Cambodia and Vietnam in the mainland Southeast Asian context, with Phnom Penh and Can Tho marked.*

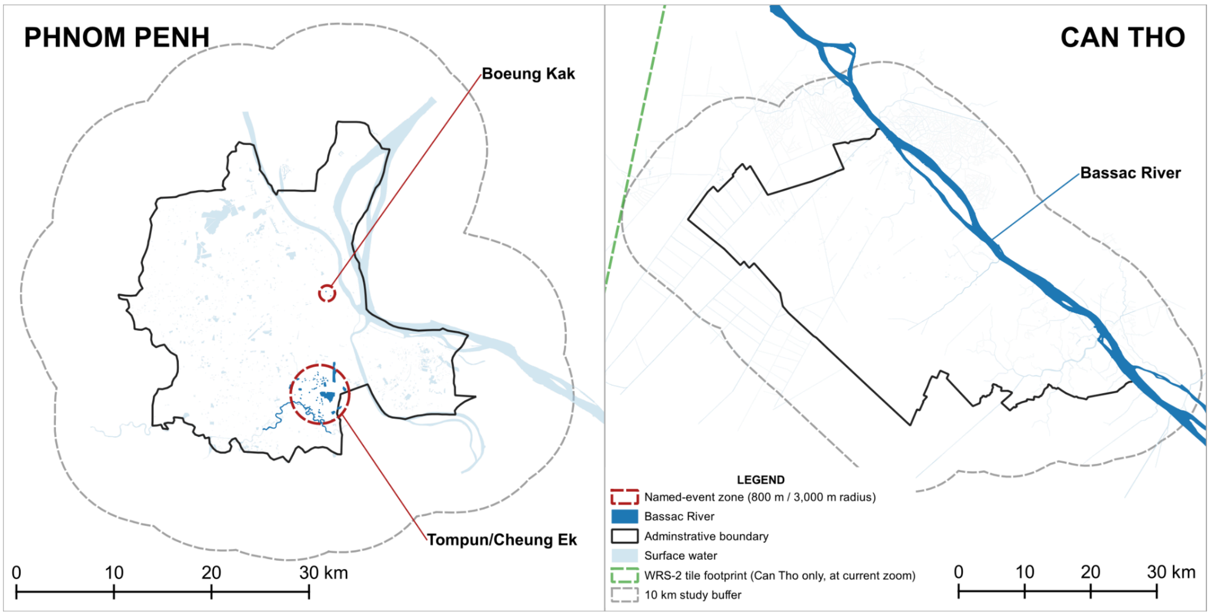

Figure 2. *Study-area extent map, two-panel (Phnom Penh; Can Tho), showing each city's administrative boundary and 10 km buffer, WRS-2 tile footprint (Path 126/Row 52; Path 125/Row 53), and named features referenced in the Results and Discussion: Boeung Kak and the Tompun/Cheung Ek wetland complex (Phnom Penh); the Bassac River corridor (Can Tho).*

3. Methodology

The study followed a three-tier analytical framework applied consistently to both cities across six anchor epochs (2000, 2005, 2010, 2015, 2020, 2024): change detection, land surface temperature (LST) attribution, and comparative synthesis. All spatial analysis used a common coordinate reference system (EPSG:32648, UTM Zone 48N) and a study extent defined by each city's administrative boundary plus a 10 km buffer. Methods M1–M10 below correspond to this framework and are reported in the order in which they were applied.

3.1 Land Surface Temperature Retrieval (M1)

Land surface temperature was derived directly from the Landsat Collection 2 Level-2 Surface Temperature (ST) product without re-derivation. Digital numbers were converted to Kelvin using the standard scale factor and offset (DN × 0.00341802 + 149.0) and to Celsius by subtracting 273.15. A physical-bounds filter (10–55°C) was applied to remove implausible pixels, attributable primarily to residual cloud and cloud-shadow contamination not fully removed by the Collection 2 QA_PIXEL CFmask.

3.2 LULC Classification — Phnom Penh (M2)

Land use and land cover for Phnom Penh was classified using a Random Forest classifier on Landsat surface reflectance bands 2–7 together with NDVI, NDWI and NDBI, applied independently to each of the six anchor epochs. Four classes were defined: water, built-up, vegetation and bare/transitional. Training points were hand-labelled from true-colour composites, cross-referenced against contemporary basemap imagery.

Point-based test accuracy exceeded 90% for most epochs but was found not to guarantee full-raster classification quality. An initial full-raster classification for the 2020 epoch produced an implausibly high built-up fraction (45.5%) against a JRC Global Human Settlement Layer (GHSL) GHS-BUILT-S cross-check of approximately 3.9%. This arose because hand-labelled training points tended to be placed in spectrally unambiguous locations, under-representing the extensive bare/built-up transitional pixels that dominate the peri-urban fringe. A boundary-correction procedure was therefore adopted as standard practice for all six epochs: classify the full raster; cross-check the built-up fraction against GHS-BUILT-S; visually inspect the result; generate spectrally-targeted boundary-candidate points for manual review where discrepancies were found; relabel and reclassify; and repeat until the result stabilised. This procedure slightly reduced point-based test accuracy in some epochs (e.g. from 97.2% to 93.7% for 2020) while producing a more representative and defensible full-raster map — a reduction in reported accuracy that reflects greater honesty about genuine classification difficulty rather than a decline in map quality. Two epochs (2010, GHS-BUILT-S ratio 3.52×; 2020, GHS-BUILT-S ratio 1.61×) required multiple correction rounds and were accepted, after diminishing returns, with documented residual built-up/bare boundary uncertainty.

3.3 LULC Classification — Can Tho (M3)

The same Random Forest approach was applied to Can Tho with an additional paddy/cropland class (five classes in total). Can Tho's land cover proved structurally harder to classify than Phnom Penh's for two compounding reasons. First, paddy exhibits a bimodal spectral signature within a single dry-season composite, because staggered triple-cropping in the Mekong Delta means actively-growing parcels (high NDVI) and dormant or recently-harvested parcels (low NDVI, spectrally close to bare soil) coexist at the same acquisition date. Second, smallholder plots in the delta are frequently smaller than the 30 m Landsat pixel, producing a genuine landscape-scale mixed-pixel problem rather than a purely spectral-index limitation.

Spectral indices alone (NDVI, NDWI, SWIR1) could not reliably separate actively-growing paddy from orchard or garden vegetation, since both present high NDVI. An operational field-geometry rule was adopted instead: parcels presenting as long, parallel strip or ridge patterns (locally “vườn”, raised-bed garden or orchard plots between drainage canals) were labelled vegetation, while open, flat, rectangular blocks were labelled paddy, cross-referenced against basemap imagery. This rule, combined with the boundary-correction workflow described in Section 3.2, was applied to all six epochs following correction of a validation error described below.

A cross-check error was identified during preparation of this study: the classified-paddy validation ratio against GlobalRice500 (500 m annual paddy-presence product) had been computed using the raw, unclipped GlobalRice500 extent (approximately 28,700 km²) rather than the true Landsat-derived study-area extent (approximately 19,200 km²), a denominator mismatch of roughly 50%. All six previously-computed paddy validation ratios were consequently invalid and were recomputed with GlobalRice500 clipped to the exact LULC raster bounding box. Built-up validation against GHS-BUILT-S was unaffected by this particular denominator error, since both quantities were computed over the same study-area geometry as it was understood at the time; that shared geometry was, however, itself later found to be incorrect for a separate reason (see below), so the built-up ratios required independent correction as well. The corrected paddy results are summarised in Table 6.

Table 6. *Can Tho LULC classification (M3) accuracy and validation summary across six anchor epochs, following correction of the GlobalRice500 cross-check extent error.*

Epoch	Test accuracy	CV accuracy	Built-up : GHS-BUILT-S ratio	Paddy : GlobalRice500 ratio
2000	84.2%	80.0%	0.72×	1.17×
2005	76.4%	78.3%	0.21×	1.05×
2010	78.9%	77.8%	0.82×	1.04×
2015	84.1%	86.2%	0.77×	1.07×
2020	87.3%	86.7%	0.98×	1.14×
2024	83.7%	76.7%	1.04×	1.12×

A second, independent correction was subsequently required: the administrative boundary used to define the Can Tho study area throughout Phases 2–4 was found to be Vietnam's post-2025 merged Can Tho–Hậu

Giang–Sóc Trăng provincial entity (6,360.82 km²) rather than the historical, pre-merger city (1,438.65 km²) the study was designed around, because the boundary file's single 'Can Tho city' row matched the merged unit without this being apparent at the time. All Can Tho rasters were re-clipped to the correct pre-merger boundary (GADM v4.1, GID_1='VNM.12_1', buffered to 3,566.01 km²) and all full-raster statistics recomputed; the values in Table 6 and elsewhere in this section reflect the corrected boundary. Corrected paddy ratios cluster between 1.04× and 1.17×, consistently above 1.0, and are independently corroborated by a convergent-shape validation (Figure 3), in which classified paddy area and the corrected GlobalRice500 series both plateau across 2000–2015 before declining sharply to 2024, despite being derived from wholly independent methods. Point-based test accuracy for Can Tho ranged from 76.4% to 87.3% across the six epochs, lower than Phnom Penh's, consistent with the structural classification difficulty described above; this is reported as an expected limitation of single-date optical classification applied to a multi-cropping agricultural landscape rather than a workflow defect.

None of the six epochs were independently blind-validated (re-checked on a random sample with no target ratio visible), with the partial exception of the 2005 and 2010 epochs' paddy points, which were spatially cross-checked against the GlobalRice500 extent; the possibility of some residual anchoring toward a ratio near 1.0 cannot be fully excluded and is disclosed here for transparency. Built-up:GHS-BUILT-S ratios have also now been recomputed against the corrected boundary, and differ substantially from the pre-correction values shown in earlier drafts. The original built-up cross-check compared classified extent against an unclipped GHS-BUILT-S export that had itself been generated using the incorrect, merged-province boundary; both quantities were therefore computed over the same oversized extent, and the resulting near-unity ratios did not constitute a meaningful validation. Once both are clipped to the corrected historical boundary, built-up area is substantially under-predicted relative to GHS-BUILT-S in every epoch through 2015 (0.21×–0.82×), most severely in 2005 (0.21×), converging to near-parity by 2020 (0.98×) and 2024 (1.04×). The severity of the 2005 under-prediction is plausibly linked to that epoch's documented residual cloud speckle across roughly the lower two-thirds of the study extent, which restricted training-point placement to the upper third/half of the raster and likely left the classifier under-exposed to built-up examples elsewhere in the scene; this is offered as a plausible contributing factor rather than a confirmed cause, since alternative explanations have not been systematically tested. This is a genuine, previously undetected limitation of the early-epoch Can Tho built-up classification, distinct from the boundary and GlobalRice500 corrections described above, and should be reported as such in the manuscript's Results and Discussion.

3.4 Change Detection (M4)

Post-classification comparison was performed across the six epochs for both cities, generating transition matrices for each consecutive epoch pair and for the direct 2000–2024 interval. Water-to-built-up transitions (Phnom Penh) and paddy-to-built-up transitions (Can Tho) were isolated as the primary conversion signal for RQ1 and RQ2 respectively (Table 7).

Table 7. *Direct 2000–2024 land-cover conversion signal (M4): converted area and percentage of 2000 baseline extent, for the water-to-built-up (Phnom Penh) and paddy-to-built-up (Can Tho) transitions.*

City (conversion type)	Converted area, 2000–2024 (km²)	% of 2000 baseline extent
Phnom Penh (water → built-up)	4.63	3.19%
Can Tho (paddy → built-up)	104.69	3.73%

Can Tho's period-by-period paddy-to-built-up conversion rate did not follow a simple rise-then-decline shape: it jumped sharply from 0.19% (2000–2005) to 2.39% (2005–2010, the strongest single period; see Section 4.2.1 for a caveat on this figure), then fluctuated at a lower but still-elevated level through 2010–2015 (1.78%), 2015–2020 (2.01%) and 2020–2024 (1.55%). Notably, the 2005–2010 spike in gross conversion did not immediately translate into a net decline in the paddy stock: the full-raster paddy percentage was essentially unchanged across this period (80.4% in 2005 versus 80.3% in 2010, Section 3.3), because comparable areas of other classes converted back into paddy over the same interval. The cumulative stock effect of sustained conversion only becomes visible from 2015 onward, when the paddy percentage falls from a plateau of roughly 80% (2000–2015) to 76.4% (2020) and 71.8% (2024).

Independent corroboration of this two-stage pattern (early gross churn without net stock change, followed by a later net decline) is shown in Figure 3, which compares classified paddy area against the corrected GlobalRice500 reference product.

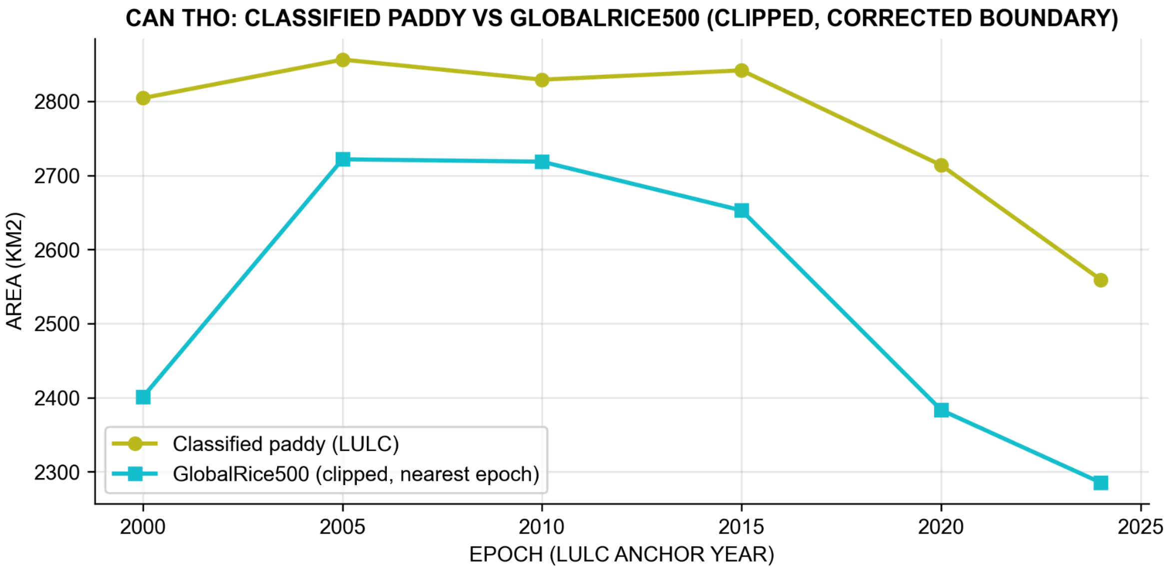

Figure 3. *Classified paddy area (Can Tho LULC, M3) versus the GlobalRice500 reference product, both clipped to the exact study-area extent, across six anchor epochs (nearest-epoch matched: GlobalRice500 years 2001, 2005, 2010, 2015, 2020 and 2022 against LULC epochs 2000, 2005, 2010, 2015, 2020 and 2024 respectively). Both independently-derived series show the same plateau across 2000–2015, followed by a marked decline to 2024.*

3.5 LST Anomaly and Reference Zone Matching (M5/M6)

Converted zones (contiguous, 8-connected clusters of pixels transitioning from water or paddy to built-up between the earliest and latest epoch compared, minimum 5 pixels / 4,500 m²) were identified for both cities. Each converted zone was matched to a contemporaneous, spatially proximate reference zone (pixels unconverted at both compared epochs) using a radius-expanding nearest-neighbour spatial search combined with covariate matching on elevation, slope, distance to city centre and aspect, derived from a 30 m SRTM digital elevation model. A difference-in-differences (DiD) design was used to isolate the LST effect attributable specifically to conversion, separating it from general background warming: the DiD-corrected mean anomaly was 7.13°C for Phnom Penh (naive estimate 11.05°C) and 0.55°C for Can Tho (naive estimate 0.37°C).

For Phnom Penh, converted zones were further attributed to two documented infilling events: Boeung Kak (11.57774°N, 104.90897°E) and a combined Tompun/Cheung Ek wetland complex (11.4844°N, 104.9022°E), the latter treated as a single continuous system on the basis of documentary evidence that the two water bodies are contiguous rather than separable. Boeung Kak zones showed no converted area before 2005, appeared during the 2005–2015 window, consistent with the documented 2007–2011 infilling period, and returned to zero converted area thereafter, providing an independent validation check on the change-detection pipeline; Boeung Kak also showed the largest DiD anomaly of any category (9.7–14.5°C). No comparably documented discrete events exist for Can Tho; conversion there was instead characterised using the ten largest converted clusters by area in each period, which together accounted for 4.6–28.4% of total converted area per period (the upper end of this range reflects 2000–2005, the period with the smallest total converted area, 3.32 km², and is correspondingly more sensitive to a handful of large zones), or 14.2% for the direct 2000–2024 interval (n=4,086 matched zones). While somewhat more concentrated than the pre-correction estimate, this remains well short of Phnom Penh's discrete, named-event pattern. The underlying result, that Can Tho's urbanisation is comparatively diffuse rather than driven by a small number of dominant clusters, still holds.

3.6 Trend Analysis (M7)

The Mann-Kendall non-parametric trend test was applied to the LST time series for four zone categories (converted, reference, urban core, background rural) in both cities. Because the study's anchor epochs are not evenly spaced (the 2020–2024 interval spans four years against five years for all other intervals), the Sen's slope estimator returned by the standard *pymannkendall* implementation, which assumes even spacing, differed by a factor of approximately five from a slope manually recomputed using true year-pair differences (Theil-Sen on actual calendar years); only the manually corrected slope is reported in this study. The corrected slope was computed as the median of the pairwise slopes (LST_j − LST_i) / (year_j − year_i) across all epoch pairs $i < j$, using each epoch's actual calendar year rather than its sequential index position, which corrects for pymannkendall's default assumption of uniform one-unit spacing between consecutive epochs (masking the four-year 2020–2024 gap against five-year gaps elsewhere).

3.7 Spatial Spillover / Buffer Analysis (M8)

Mean LST was computed within concentric distance bins (0–100 m, 100–250 m, 250–500 m, 500–1,000 m, and >1,000 m) around converted zones at the final epoch, using a single-pass Euclidean distance transform rather than per-zone circular buffers for computational efficiency. For Can Tho, this produced a clean, monotonic decay from the converted-zone edge to background level by approximately 250–500 m. For Phnom Penh, an initial analysis produced an inverted pattern (LST cooler near converted zones than far), traced to the proximity of Phnom Penh's converted zones to surviving water bodies within the same wetland systems; excluding water pixels from the ring means recovered the expected pattern, with anomaly peaking near the zone edge and decaying to near-zero beyond 1,000 m, over a more gradual distance than observed in Can Tho.

3.8 Seasonal Comparison (M9)

Wet-season LST composites (May–October) were built using the same coverage-aware compositing logic as the dry-season composites (Section 3.1), for the same six anchor epochs and the same four zone categories used in Section 3.6 (converted, reference, urban core, background rural). For each category and epoch, a dry-minus-wet differential was computed. Epochs with materially degraded wet-season scene coverage were flagged as low-confidence and excluded from the headline mean differential reported in Section 4: epoch 2010 for Phnom Penh (four usable scenes, May and June entirely absent), and epochs 2010 and 2020 for Can Tho (residual cloud contamination reducing wet-season valid-pixel coverage well below the corresponding dry-season composite). Cloud-free wet-season composites are not a random sample of wet-season weather: they systematically oversample the clearest, most intensely sunny days between rain events, which can run hotter than typical wet-season conditions. This is a general limitation of any wet-season LST compositing approach, not specific to either city, and is disclosed here as a caveat on the seasonal-comparison results throughout.

3.9 Normalised Cooling Loss (RQ3 Synthesis Metric)

To enable a fair cross-city comparison of cooling-infrastructure loss per unit area (RQ3), two complementary metrics were computed from the matched converted/reference zone pairs used in Section 3.5: (a) the area-weighted mean DiD anomaly, representing per-km² thermal intensity; and (b) total thermal impact, the area-weighted mean anomaly multiplied by total converted area (units °C·km²), representing combined magnitude and extent. The two metrics were found to rank the two cities in opposite order and are therefore reported together rather than collapsed into a single figure.

3.10 Settlement Morphology Context (M10)

Each matched converted zone from Section 3.5 was additionally classified by settlement morphology using the JRC Global Human Settlement Layer Degree of Urbanisation (GHS-SMOD) product, grouped into four categories (urban, suburban/peri-urban, rural, water) and assigned using the nearest available SMOD epoch preceding each conversion period. GHS-SMOD does not extend to 2024; the 2020 layer was used as the nearest available epoch for periods requiring it.

3.11 Tools and Software

Analysis was performed in Python (*geopandas*, *rasterio*, *numpy*, *scikit-learn*, *scipy*, *pymannkendall*, *osmnx*) within Jupyter notebooks. Pre-processing, including Landsat compositing, cloud masking, and extraction of JRC Global Surface Water and GlobalRice500 data, was performed in *Google Earth Engine*. *QGIS* was used for visual inspection, training-point review, and cartographic composition of the study-area figures (Section 2.4). All classifiers used a fixed random seed for reproducibility.

4. Results

Results are reported in the order of the three research questions (Section 1.3): RQ1 (Phnom Penh, Section 4.1), RQ2 (Can Tho, Section 4.2), and RQ3, the comparative synthesis (Section 4.3). Each city-specific subsection follows the methods ordering established in Section 3 (M4 through M10). Methodological detail already given in Section 3 is not repeated here; this section reports what was found.

4.1 RQ1, Phnom Penh: Water Body Loss and Land Surface Temperature

4.1.1 Extent and Timing of Conversion

Direct water-to-built-up conversion between 2000 and 2024 totalled 4.63 km², 3.19% of the 2000 water baseline extent (Table 7, Section 3.4). Period-by-period conversion rates ranged from 0.97% to 3.75% of the period's water extent; the 2010 and 2020 epochs carry the residual built-up/bare boundary uncertainty already documented for the LULC classification (Section 3.2) and should be read with that caveat in mind.

4.1.2 LST Anomaly and Named-Event Attribution

Converted zones were matched to contemporaneous reference zones using the covariate-based design described in Section 3.5. Of the converted-zone population identified by the direct 2000–2024 comparison, 123 zones were successfully matched, with a combined area of 3.56 km², somewhat below the full 4.63 km² change-detection total; the difference reflects zones below the minimum mapping unit or without a successful covariate match, not a discrepancy between methods.

The difference-in-differences (DiD) design yielded a mean LST anomaly of 7.13°C attributable to conversion, against a naive (unadjusted) estimate of 11.05°C; the gap between the two indicates that a substantial share of the naive anomaly reflects general background warming rather than the conversion itself, which the DiD design removes.

Two documented infilling events were used to validate the change-detection pipeline independently: Boeung Kak (11.57774°N, 104.90897°E) and a combined Tompun/Cheung Ek wetland complex (11.4844°N, 104.9022°E), the latter treated as a single continuous system on documentary evidence that the two water bodies are contiguous. Boeung Kak zones showed zero converted area before 2005, appeared during the 2005–2015 window, consistent with the documented 2007–2011 infilling period, and returned to zero thereafter. This is a pattern the change-detection pipeline was not designed to reproduce, so it provides an independent check on the pipeline's validity. Boeung Kak also carried the largest DiD anomaly of any category or named event, 9.7–14.5°C across periods.

4.1.3 Long-Term Trend

The Mann-Kendall trend test (manually corrected Theil-Sen slope; Section 3.6) was applied to four zone categories across the study's six anchor epochs, a sample size that limits statistical power to detect trends where they exist (Section 5.7). Converted zones showed a significant increasing trend of 0.40°C per year ($p = 0.024$, $\tau = 0.867$, near-perfectly monotonic). Background rural zones also showed a significant increasing trend, 0.24°C per year ($p = 0.0085$, $\tau = 1.000$, perfectly monotonic across all six epochs). Neither reference nor urban-core zones reached significance ($p = 0.060$ and $p = 0.133$ respectively).

Table 8. *Mann-Kendall trend results, Phnom Penh, four zone categories (M7).*

Category	Trend	Corrected slope (°C/yr)	p-value	τ
Converted	Increasing (significant)	0.40	0.024	0.867
Reference	No trend	–	0.060	–
Urban core	No trend	–	0.133	–
Background rural	Increasing (significant)	0.24	0.0085	1.000

Note: Corrected slope and τ are not separately reported here for the reference and urban-core categories, as those values were not carried forward from the trend-analysis notebook into the working record; both are reported as 'no trend' on the p-value alone. Full values are available in mannkendall_trend_results.csv if required for the final table.

Converted zones are warming approximately 1.7 times faster than the general background rural trend ($0.40 \div 0.24 \approx 1.67$). Read alongside the DiD anomaly (Section 4.1.2), this indicates two distinct signals operating together: a real background regional warming trend across the study period, and an additional, conversion-specific anomaly on top of it.

4.1.4 Spatial Spillover

Mean LST was computed in concentric distance bins around converted zones at the final epoch (Section 3.7). An initial analysis, including water pixels in the ring means, produced an inverted pattern (cooler near converted zones than far), traced to the proximity of Phnom Penh's converted zones to surviving water bodies within the same wetland systems. Excluding water pixels from the ring calculation recovered the expected pattern: a mean anomaly of +0.99°C in the 0–100 m ring, declining to +0.04°C beyond 1,000 m, a near-complete convergence to zero background level.

4.1.5 Seasonal Modulation

Dry-season and wet-season (May–October) LST composites were compared for each zone category (Section 3.8, M9). The 2010 epoch was excluded as low-confidence, on the basis of thin wet-season scene coverage (four scenes, May and June entirely missing); 2015 was retained despite an unusual seasonal reading, attributed to the documented 2015–16 El Niño/drought event rather than a data artefact. With 2010 excluded, all four categories showed the dry season warmer than the wet season (Table 9), consistent with the expected direction of monsoonal cooling.

Table 9. *Dry-season minus wet-season LST differential, Phnom Penh, four zone categories, 2010 epoch excluded (M9).*

Category	Dry − wet differential (°C)
Converted	+0.56
Reference	+0.77

Urban core	+1.78
Background rural	+2.46

Note: Phnom Penh's wet-season composites average approximately eight scenes per epoch across the study period, compared to approximately twenty-four for Can Tho (Section 4.3.3); this smaller sample size makes the dry-minus-wet differentials reported above more susceptible to individual scene anomalies than Can Tho's equivalent figures (Table 14).

The ordering across categories is not what a simple thermal-buffering account would predict: urban-core zones show a larger dry-to-wet swing (+1.78°C) than reference water zones (+0.77°C). A plausible explanation, offered here without further testing, is that open water has high thermal inertia and does not reach as high a dry-season peak to begin with, leaving less capacity to cool further once the wet season arrives, whereas impervious surfaces run hot in the dry season with no evaporative buffering and consequently have more room to drop.

4.1.6 Settlement-Morphology Context

Matched converted zones were classified by settlement morphology (GHS-SMOD, grouped into four categories; Section 3.10, M10) using the nearest preceding SMOD epoch. The DiD anomaly by settlement class did not follow a clean urban-to-rural gradient (Table 10): rural zones showed the largest mean anomaly, but urban zones exceeded suburban/peri-urban zones, and water-context zones exceeded both urban and suburban.

Table 10. *DiD anomaly by settlement-morphology class, Phnom Penh, direct 2000–2024 (M10).*

Settlement class	Mean DiD anomaly (°C)
Rural	8.25
Water	7.76
Urban	6.45
Suburban / peri-urban	6.11

A Kruskal-Wallis test across the four classes did not reach significance ($p = 0.180$, $n = 22–36$ per group), so this pattern is reported as suggestive rather than confirmed. A check of pre-conversion baseline LST by the same settlement classes showed the same directional pattern already present before any conversion occurred, though weaker and less monotonic than Can Tho's equivalent check (Section 4.2.6). This is consistent with Phnom Penh's non-significant result here, and with the possibility that at least part of any settlement-morphology pattern in the anomaly reflects pre-existing baseline differences rather than an independent effect of settlement context on conversion impact.

Boeung Kak stands as a named exception to this pattern. All five Boeung Kak zones classify as "urban" SMOD context, yet showed large anomalies (7.3–10.9°C, exceeding even the rural-category mean of 8.25°C) despite a comparatively cool pre-conversion baseline (25.5–28.8°C, below the urban-category baseline average). A plausible reconciliation is that the aggregate settlement-morphology pattern describes typical, incremental urban-fringe conversions, which are thermally buffered by surrounding already-warm fabric, whereas Boeung Kak was a large, complete, singular infilling event that overwhelms any such buffering regardless of surrounding context, consistent with Boeung Kak already standing out as the single strongest anomaly of any named event or category (Section 4.1.2).

4.1.7 Summary Against H1

H1 (Section 1.3) proposed that former lake and wetland surfaces would show significantly higher LST, estimated at +2 to +5°C relative to pre-infilling periods, after controlling for seasonal variability. The observed DiD-corrected anomaly, 7.13°C, exceeds the upper bound of this estimate. Seasonal control in this design is achieved structurally, by comparing dry-season composites to dry-season composites at each epoch, rather than through a separate statistical adjustment; the seasonal-modulation analysis (Section 4.1.5) is a distinct, complementary line of evidence rather than a component of the DiD estimate itself. The magnitude and its relationship to the single largest contributing event, Boeung Kak, are interpreted further in the Discussion.

4.2 RQ2, Can Tho: Paddy Conversion and Land Surface Temperature

All figures in this subsection use the corrected pre-merger Can Tho boundary (Section 2.1.2); none reflect the invalid merged-province extent superseded during manuscript preparation.

4.2.1 Extent and Timing of Conversion

Direct paddy-to-built-up conversion between 2000 and 2024 totalled 104.69 km², 3.73% of the 2000 paddy baseline extent (Table 7, Section 3.4). Conversion did not proceed as a simple rise-then-decline: the period-by-period rate jumped sharply from 2000–2005 to a peak in 2005–2010, then fluctuated at a lower but still-elevated level through to 2024 (Table 11a).

Table 11a. *Paddy-to-built-up conversion rate by period, as a percentage of that period's paddy extent (M4).*

Period	Paddy → built-up (% of period paddy extent)
2000–2005	0.19%
2005–2010	2.39% (strongest period)
2010–2015	1.78%
2015–2020	2.01%
2020–2024	1.55%

The 2005–2010 spike in gross conversion did not translate into an equivalent net decline in the paddy stock: the full-raster paddy percentage was essentially unchanged across that period (Table 11b), because comparable areas of other classes converted back into paddy over the same interval. The cumulative effect of sustained conversion only becomes visible in the stock trajectory from 2015 onward. This period-by-period pattern should be read against a limitation already noted for the underlying classification (Section 3.3): built-up area was under-predicted relative to GHS-BUILT-S across the early epochs, most severely in 2005 (0.21×), before recovering toward near-parity by 2010 (0.82×) and later epochs. Because the 2005 classifier under-detected genuine built-up pixels, part of the apparent 2005–2010 conversion spike is likely a classification-recovery artefact rather than physical conversion: pixels present as built-up but misclassified as bare or paddy in 2005 would be correctly identified once classification quality improved, registering in the transition matrix as new conversion regardless of whether land cover actually changed in that interval. The same mechanism plausibly deflates the 2000–2005 rate in the opposite direction. The direct 2000–2024 headline total (104.69 km², Table 7) is not immune either, since 2000's own built-up ratio (0.72×) also falls short of 2024's (1.04×), though to a lesser degree than the intermediate distortion; the true magnitude of this effect has not been separately quantified, and the period-by-period rates in particular should be read as bounds shaped partly by this confound rather than purely physical signals.

Table 11b. *Full-raster classified paddy extent by epoch, as a percentage of the valid study-area extent (M3).*

Epoch	Full-raster paddy (% of valid extent)
2000	79.93%
2005	80.38%
2010	80.29%
2015	79.76%
2020	76.41%
2024	71.77%

This two-stage pattern (early gross churn without net stock change, followed by a later net decline) is corroborated by the independent GlobalRice500 validation series (Figure 3, Section 3.4), which shows the same plateau across 2000–2015 followed by a decline to 2024, despite being derived from a wholly independent method.

4.2.2 LST Anomaly and Cluster-Based Characterisation

Of the converted-zone population identified by the direct 2000–2024 comparison, 4,086 of 4,100 zones were successfully matched to reference zones, with a combined area of 80.01 km². The DiD design yielded a mean LST anomaly of 0.55°C attributable to conversion, against a naive (unadjusted) estimate of 0.37°C. This is the reverse of the Phnom Penh pattern (Section 4.1.2), where the naive estimate exceeded the DiD-corrected figure; for Can Tho, adjusting for background warming trends increases rather than decreases the estimated conversion-attributable anomaly.

No comparably documented discrete infilling events exist for Can Tho, so conversion was instead characterised using the ten largest converted clusters by area in each period. These accounted for 4.6–28.4% of total converted area per period (the upper end reflecting 2000–2005, the period with the smallest total converted area and correspondingly the most sensitive to a handful of large zones), or 14.2% for the direct 2000–2024 interval (11.35 km² of 80.01 km², across 4,086 matched zones). Unlike Phnom Penh, where a small number of large, discrete, named events account for the bulk of the signal (Section 4.1.2), Can Tho's urbanisation pattern is not dominated by a small number of large clusters.

4.2.3 Long-Term Trend

The Mann-Kendall trend test was applied to the same four zone categories used for Phnom Penh (Section 3.6). None reached significance (Table 12).

Table 12. *Mann-Kendall trend results, Can Tho, four zone categories (M7).*

Category	Trend	Corrected slope (°C/yr)	p-value	τ
Converted	No trend	0.1018	0.2597	0.4667
Reference	No trend	0.0766	1.0000	0.0667
Urban core	No trend	−0.0012	1.0000	−0.0667
Background rural	No trend	0.0101	0.7071	0.2000

Converted zones carry the highest τ of the four categories (0.4667), directionally consistent with warming, but this does not reach significance and is reported as suggestive rather than confirmed. The background-rural sample is small following the boundary correction (10.89 km², Section 3.5), a disproportionate reduction relative to the other categories that makes this category's representativeness a more pressing caveat than it was before the correction.

4.2.4 Spatial Spillover

Mean LST was computed in the same concentric distance bins used for Phnom Penh (Section 3.7), relative to the background-rural reference category (mean 31.69°C at the 2024 epoch). Unlike Phnom Penh, no water-exclusion correction was required for Can Tho: the ring means show a clean, monotonic decay from the converted-zone edge outward (Table 13), reaching near-background level by 100–250 m.

Table 13. *Mean LST anomaly by distance ring, relative to the background-rural reference category, Can Tho, 2024 (M8).*

Distance ring	Mean LST anomaly vs. background-rural reference (°C)

0–100 m	+1.677
100–250 m	+0.332
250–500 m	−0.403
500–1,000 m	−0.907
>1,000 m (background)	−1.160

4.2.5 Seasonal Modulation

Dry-season and wet-season composites were compared for each zone category (Section 3.8, M9). Epochs 2010 and 2020 were excluded as low-confidence, on the basis of residual wet-season cloud contamination (Section 3.8). With these two epochs excluded, all four categories showed the wet season warmer than the dry season (Table 14), the reverse of the direction seen for Phnom Penh (Section 4.1.5).

Table 14. *Dry-season minus wet-season LST differential, Can Tho, four zone categories, 2010 and 2020 epochs excluded (M9).*

Category	Dry − wet differential (°C)
Converted	−2.21
Reference	−2.14
Urban core	−3.45
Background rural	−1.72

The reference category in this comparison is unconverted paddy, and its wet/dry differential should not be read as the behaviour of a uniformly flooded field. Can Tho practises staggered triple-cropping, so at any single wet-season satellite pass, the reference paddy population is a mixture of flooded/growing, draining, recently-harvested and short-fallow parcels rather than a single, consistent land-cover state; this is the same bimodal cropping pattern already noted for the LULC classification (Section 3.3) and should be borne in mind when interpreting this category's seasonal signal.

4.2.6 Settlement-Morphology Context

Matched converted zones were classified by settlement morphology (Section 3.10, M10). Unlike Phnom Penh, the pattern here is both statistically and, given its magnitude relative to the headline DiD anomaly, practically significant: DiD anomaly decreases monotonically from rural to urban context (Table 15), and a Kruskal-Wallis test across the three classes with adequate sample size (water, $n = 1$, was excluded) was highly significant ($H = 45.386$, $p < 0.0001$). All three pairwise comparisons (Bonferroni-corrected $\alpha = 0.0167$) were significant: rural vs. suburban/peri-urban ($p < 0.0001$), rural vs. urban ($p < 0.0001$), and suburban/peri-urban vs. urban ($p = 0.0010$).

Table 15. *DiD anomaly and pre-conversion baseline LST by settlement-morphology class, Can Tho, direct 2000–2024 (M10).*

Settlement class	n	Mean DiD anomaly (°C)	Pre-conversion baseline LST (°C)
Rural	759	1.186	32.81
Suburban / peri-urban	2,075	0.598	33.65
Urban	1,228	0.114	34.85

Pre-conversion baseline LST follows the same monotonic pattern by settlement class, and the baseline gap between rural and urban zones (2.04°C) exceeds the anomaly gap between the same two classes (1.07°C). This indicates that the settlement-morphology pattern in the DiD anomaly is at least substantially, and possibly fully, attributable to pre-existing baseline temperature differences rather than an independent effect of settlement context on conversion impact; settlement morphology in this reading corroborates the spillover finding in Section 4.2.4 (proximity to existing built-up heat) rather than constituting a separate driver. The rural-to-urban anomaly gap (1.07°C) is itself larger than Can Tho's entire headline DiD anomaly (0.55°C, Section 4.2.2), so this is not a large-sample artefact of the kind that requires the caution applied elsewhere to some other Can Tho findings; the gap is both statistically and practically substantial.

4.2.7 Summary Against H2

H2 (Section 1.3) proposed that peri-urban zones in Can Tho where paddy fields have been converted to built-up land would show a measurable LST increase, estimated at +1.5 to +3°C, relative to unconverted paddy reference zones. The observed DiD-corrected anomaly, 0.55°C, falls well below the lower bound of this estimate. This contrasts with Phnom Penh, where the equivalent comparison against H1 (Section 4.1.7) exceeded its hypothesised upper bound rather than falling short of it. Both departures from their respective hypothesised ranges are interpreted further in the Discussion.

4.3 RQ3: Comparative Synthesis

The preceding subsections deliberately reported each city's results without cross-city comparison, so that each stood on its own evidence. This subsection brings the two together to address RQ3: whether the two cities show systematically different LST outcomes, and what that reveals about which category of cooling infrastructure carries the higher thermal risk when removed.

4.3.1 Normalised Cooling Loss

Two complementary metrics were computed from the same direct 2000–2024 matched-zone data used in Sections 4.1.2 and 4.2.2 (Section 3.9): Option A, the area-weighted mean DiD anomaly, representing true per-km² thermal intensity; and Option B, total thermal impact, the area-weighted mean anomaly multiplied by total converted area, representing combined magnitude and extent (Table 16).

Table 16. *Normalised cooling loss, both cities, direct 2000–2024 (Section 3.9).*

Metric	Phnom Penh	Can Tho
Matched zones (direct 2000–2024)	123	4,086
Total converted area (km²)	3.56	80.01
Unweighted mean anomaly (°C)	7.129	0.553
Area-weighted mean anomaly, Option A (°C)	9.409	1.330
Total thermal impact, Option B (°C·km²)	33.53	106.44

The two metrics rank the cities in opposite order. By intensity (Option A), Phnom Penh's per-km² anomaly (9.409°C) is roughly seven times Can Tho's (1.330°C). By total impact (Option B), Can Tho's converted extent (80.01 km², over twenty times Phnom Penh's 3.56 km²) more than offsets its lower per-unit intensity, giving Can Tho the larger total thermal impact (106.44 vs. 33.53 °C·km²).

4.3.2 Structural Contrast: Concentrated Versus Diffuse Urbanisation

Three independent lines of evidence, drawn from different analyses, converge on the same structural contrast between the two cities. First, cluster dominance. Phnom Penh's conversion signal is dominated by a small number of large, discrete, documented events; Boeung Kak alone carried the largest DiD anomaly of any category (Section 4.1.2). Can Tho's ten largest clusters account for only 14.2% of total converted area in the direct 2000–2024 comparison (Section 4.2.2); the top 10 clusters (11.35 km²) carry a mean anomaly of 2.735°C, against 0.548°C for the remaining 4,076 matched zones (68.66 km²), a ratio of approximately 5.0.

Second, the relationship between zone area and anomaly magnitude across each city's full matched-zone population. For Phnom Penh, a Spearman correlation between zone area and DiD anomaly returned $r = 0.308$ ($p = 0.0005$, $n = 123$), a genuine, moderate, broad relationship consistent with the Boeung Kak pattern in which large, complete conversions run hottest. For Can Tho, the equivalent correlation returned $r = 0.058$ ($p = 0.0002$, $n = 4{,}086$). The p-value alone would suggest significance, but $r^2 \approx 0.003$ means zone area explains only around 0.3% of the variance in anomaly magnitude; with a sample this large, a p-value this small is not, by itself, evidence of a meaningful relationship, and it is not treated as such here.

Third, spillover shape (Sections 4.1.4, 4.2.4). Phnom Penh's buffer anomaly decays gradually, reaching near-zero only beyond 1,000 m; Can Tho's buffer anomaly decays sharply, reaching near-background level by 100–250 m. A more gradual decay is consistent with converted zones embedded within, or adjacent to, broader contiguous systems (the wetland complexes from which Phnom Penh's converted zones are drawn); a sharper decay is consistent with converted zones more sharply bounded against surrounding unconverted land, as the diffuse, many-small-conversions pattern in Can Tho would predict.

Together, these three lines of evidence describe a consistent structural difference in how each city loses cooling infrastructure: Phnom Penh's loss is concentrated in a small number of large, government-negotiated infilling events; Can Tho's is diffuse, accumulated from many small, independent conversions distributed across the peri-urban fringe.

4.3.3 Seasonal Modulation: A Sign Flip

Sections 4.1.5 and 4.2.5 reported, for each city separately, which season runs warmer. Read together, the two cities show a complete sign flip rather than a difference of degree: Phnom Penh is warmer in the dry season across all four zone categories (+0.56 to +2.46°C, dry minus wet); Can Tho is warmer in the wet season across all four categories (−1.72 to −3.45°C, dry minus wet).

Two candidate explanations were tested and set aside. LULC misclassification could plausibly add noise to either city's seasonal signal, but is not a parsimonious explanation for a full sign flip, since that would require classification bias to run in opposite directions in the two cities, a larger coincidence than ordinary classification noise. Wet-season scene-timing skew, the possibility that one city's wet-season composites are drawn from systematically earlier or later parts of the monsoon than the other's, was tested directly against Earth Engine scene-acquisition dates: Phnom Penh's wet-season scenes ($n = 50$) were 36.0% May–June and 30.0% September–October; Can Tho's ($n = 146$) were 38.4% and 33.6% respectively, a nearly identical seasonal distribution between the two cities. This rules out scene-timing skew as the explanation.

That check did surface a genuine, separate caveat: Can Tho has roughly three times as many wet-season scenes per epoch, on average, as Phnom Penh ($146 \div 6 \approx 24$ versus $50 \div 6 \approx 8$), consistently across the record. This means Phnom Penh's wet-season composites generally rest on thinner data than Can Tho's, warranting broader caution about the Phnom Penh seasonal results specifically, not only the epochs already excluded as low-confidence.

With both tested explanations ruled out, the leading explanation for the sign flip, reached by elimination rather than direct confirmation, is a genuine regional climatic or geographic difference between the two cities: different immediate geography (Phnom Penh, a river-confluence basin; Can Tho, a flat, low-lying delta), and a structurally different reference land cover (Phnom Penh's reference category is open river and lake water, which does not follow a farming calendar; Can Tho's is staggered-cropping paddy, whose wet-season state is itself a mixture of flooded, transitional and dry-harvested parcels, Section 4.2.5). This explanation is offered as the most likely account given what has been ruled out, not as a confirmed mechanism, and is examined further in the Discussion.

4.3.4 Settlement Morphology: Convergent Corroboration

Sections 4.1.6 and 4.2.6 each tested whether settlement-morphology context (GHS-SMOD class) modulates the DiD anomaly, and each checked whether the same pattern already existed in the pre-conversion baseline. The two cities differ in statistical strength: Phnom Penh's settlement-class pattern did not reach significance ($p = 0.180$) and was less monotonic; Can Tho's did ($p < 0.0001$, all pairwise comparisons significant) and was cleanly monotonic. Despite this difference in strength, both cities point toward the same underlying interpretation. In both, the pre-conversion baseline LST already varies by settlement class in the same direction as the anomaly, and for Can Tho, where the comparison is precise enough to state numerically, the baseline gap between rural and urban zones (2.04°C) exceeds the anomaly gap between the same two classes (1.07°C, Section 4.2.6). This indicates that settlement morphology, in both cities, is likely acting substantially as a coarse, discrete proxy for the same proximity-to-existing-heat mechanism already measured directly and continuously by the buffer-spillover analysis (Sections 4.1.4, 4.2.4), rather than constituting an independent driver of conversion impact. Phnom Penh's named exception to its own aggregate pattern, Boeung Kak (Section 4.1.6), is consistent with this reading: a single, complete, large-scale event can overwhelm the buffering that the aggregate pattern otherwise describes for typical, incremental conversions.

4.3.5 Summary Against H3

H3 (Section 1.3) proposed that the per-unit-area thermal consequence of water body loss (Phnom Penh) would exceed that of paddy loss (Can Tho), reflecting the greater latent heat flux of open water relative to periodically flooded agricultural land. H3 is phrased explicitly in per-unit-area terms, which corresponds most directly to Option A in Section 4.3.1: by that measure, Phnom Penh's intensity (9.409°C) substantially exceeds Can Tho's (1.330°C), supporting H3 as stated. The total-impact measure (Option B) tells a different story, in which Can Tho's much larger converted extent gives it the greater aggregate thermal impact. Both readings are correct for what they measure; which one is the more policy-relevant answer to “which category of natural cooling resource represents the higher thermal risk when removed” is a question of framing rather than of data, and is taken up in the Discussion.

5. Discussion

5.1 Principal Findings and Land-Cover Change Context

The two cities lost cooling infrastructure in ways that differed in almost every respect examined by this study. Phnom Penh's water-body loss produced a large, DiD-corrected LST anomaly (7.13°C, Section 4.1.2), concentrated in a small number of large, documented infilling events. Can Tho's paddy loss produced a much smaller anomaly (0.55°C, Section 4.2.2), accumulated diffusely across thousands of small, independent conversions. Both departed from their respective pre-registered hypotheses, in opposite directions: Phnom Penh's anomaly exceeded H1's upper bound, and Can Tho's fell short of H2's lower bound. Sections 5.2 to 5.6 take each major finding in turn; Section 5.7 sets out the study's limitations; Section 5.8 identifies specific candidates for future work.

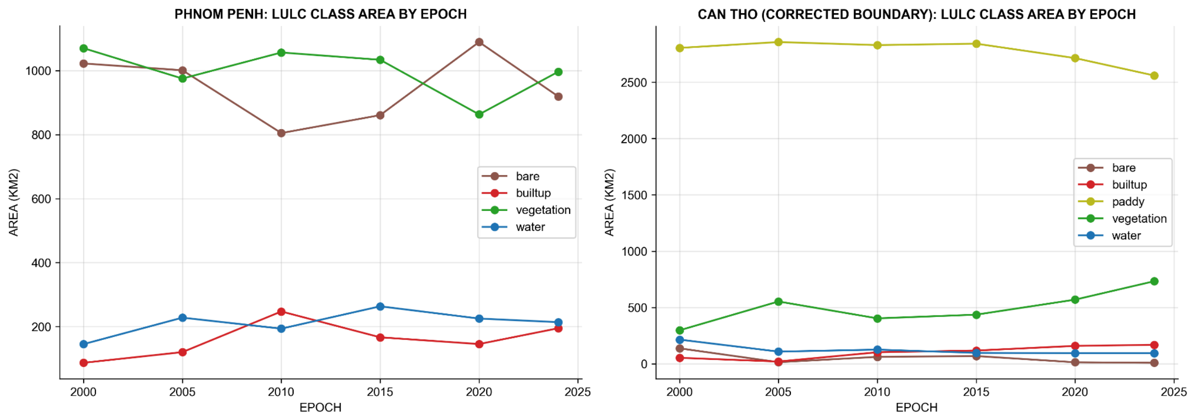

Figure 4. *Classified land-cover class area by epoch, two-panel (Phnom Penh; Can Tho), 2000–2024. Can Tho's paddy trajectory corresponds to Table 11b (Section 4.2.1); Phnom Penh's built-up growth is the land-cover counterpart to the water-loss trajectory reported in Section 4.1.1.*

5.2 Evaluation of Hypotheses

H1 proposed a Phnom Penh LST anomaly of +2 to +5°C. The observed DiD-corrected anomaly, 7.13°C, exceeds this range by a margin of over 2°C above the upper bound (Section 4.1.7). Two considerations bear on why. First, H1's estimated range was drawn from published studies in comparable tropical urban contexts (Section 1.3), not from a design that specifically isolates a conversion-attributable anomaly from background warming via difference-in-differences; a naive, non-DiD estimate of the same Phnom Penh signal was 11.05°C (Section 4.1.2), further from the hypothesised range still, so the DiD correction narrows the gap without closing it. Second, the headline figure is substantially influenced by Boeung Kak, whose DiD anomaly (9.7–14.5°C, Section 4.1.2) is the largest of any category or event and pulls the overall mean upward; Boeung Kak was a large, complete, singular, government-negotiated infilling event, and may not be representative of the more incremental water-body losses the hypothesised range was implicitly calibrated to.

Placed against published urban water-body cooling literature from Chinese cities, Phnom Penh's result is large but not without precedent. Xie et al. (2023), surveying urban water bodies in Wuhan, reported a mean cooling intensity of 5.5°C with a range of 1.1 to 13.3°C; Cai et al. (2022), comparing 34 Chinese megacities, reported a maximum cooling intensity ranging from −2.21 to 7.83°C depending on city-water layout. Phnom Penh's headline anomaly (7.13°C) falls within both reported ranges, above the Wuhan mean and near the upper end of the 34-city comparison; Boeung Kak specifically (9.7–14.5°C) exceeds the 34-city study's upper bound but remains within the wider Wuhan range. This places Phnom Penh's result within the envelope of what has been reported for other rapidly urbanising cities with substantial water-body loss, rather than as an outlier requiring a mechanism beyond those already documented in that literature.

H2 proposed a Can Tho LST increase of +1.5 to +3°C. The observed DiD-corrected anomaly, 0.55°C, falls well below this range, on the opposite side from Phnom Penh's departure from H1. Read against a second reference point, however, the result looks different: Weng et al. (2026) established a global paddy evapotranspirative cooling effect of only 0.21–0.27°C (Section 1.2), and Can Tho's measured anomaly is between roughly 2.0 and 2.6 times this global baseline, depending which end of Weng et al.'s range is used. H2's hypothesised range, like H1's, was drawn from comparable tropical urban contexts in the general built-up-conversion literature (Section 1.3) rather than calibrated specifically to the smaller paddy-evapotranspiration cooling effect that Gap 1 (Section 1.2) identifies as the mechanism being lost. Measured against that more specific baseline rather than against the general urban-conversion literature the hypothesis range drew on, Can Tho's result is not small: it is a multiple of the effect it is meant to be losing. This reframing does not correct H2, which is evaluated against its own stated terms and falls short of them, but it does suggest that the shortfall may partly reflect where the hypothesised range was drawn from rather than a genuinely negligible effect of paddy conversion on LST.

H3 proposed that the per-unit-area thermal consequence of water-body loss would exceed that of paddy loss. This is supported when "per-unit-area thermal consequence" is read as intensity (Option A, Section 4.3.1): Phnom Penh's 9.409°C is roughly seven times Can Tho's 1.330°C, consistent with H3's stated mechanism, the greater latent heat flux of open water relative to periodically flooded agricultural land. It is not supported when read as total impact (Option B): Can Tho's 106.44°C·km² exceeds Phnom Penh's 33.53°C·km² by a factor of roughly three, because Can Tho's much larger converted extent (Section 4.3.1) more than offsets its lower per-unit intensity. H3 is, in this sense, a claim about physical mechanism that this study's intensity measure supports; whether it is also the more policy-relevant answer to which resource represents the higher thermal risk depends on how much of each resource a given city stands to lose, which is an empirical fact about urbanisation pattern (Section 5.4) rather than a property of the land-cover type itself.

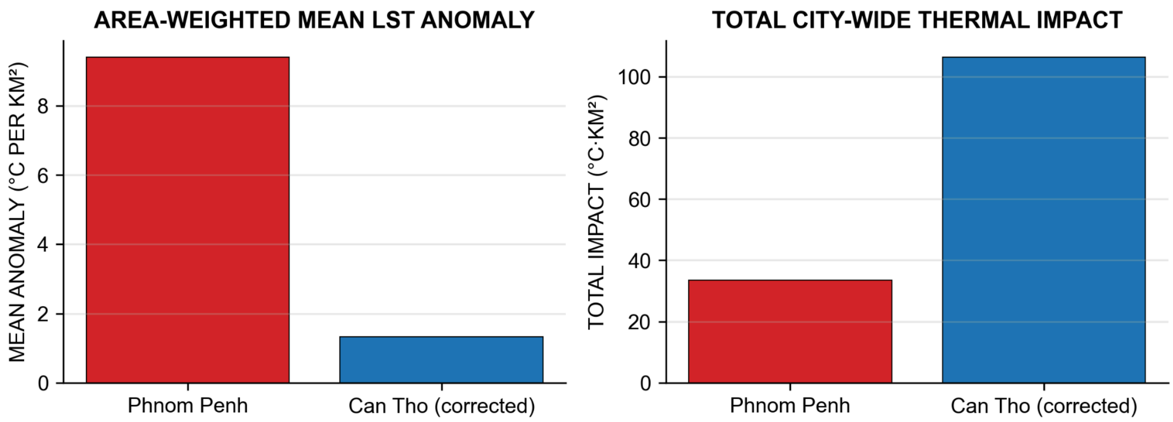

Figure 5. *Normalised cooling loss, two-panel (Option A, area-weighted intensity; Option B, total thermal impact), both cities, direct 2000–2024. Corresponds to Table 16, Section 4.3.1.*

5.3 Long-Term Trend in Context

Phnom Penh showed significant long-term warming in both converted zones (0.40°C/yr) and background rural zones (0.24°C/yr), with converted zones warming approximately 1.7 times faster (Section 4.1.3). This indicates two distinct signals operating together in Phnom Penh: a real regional warming trend across the study period, and an additional, conversion-specific anomaly superimposed on it. Can Tho showed no significant trend in any of the four zone categories (Section 4.2.3), though converted zones carried the highest τ (0.4667) of the four, directionally consistent with warming. Whether this reflects a genuine absence of a Can Tho long-term trend, greater noise in the Can Tho LST time series from the data-quality issues catalogued in Section 5.8, or reduced statistical power following the post-correction contraction of the background-rural sample (10.89 km², Section 4.2.3) cannot be distinguished with the data available, and is left as an open question rather than resolved here.

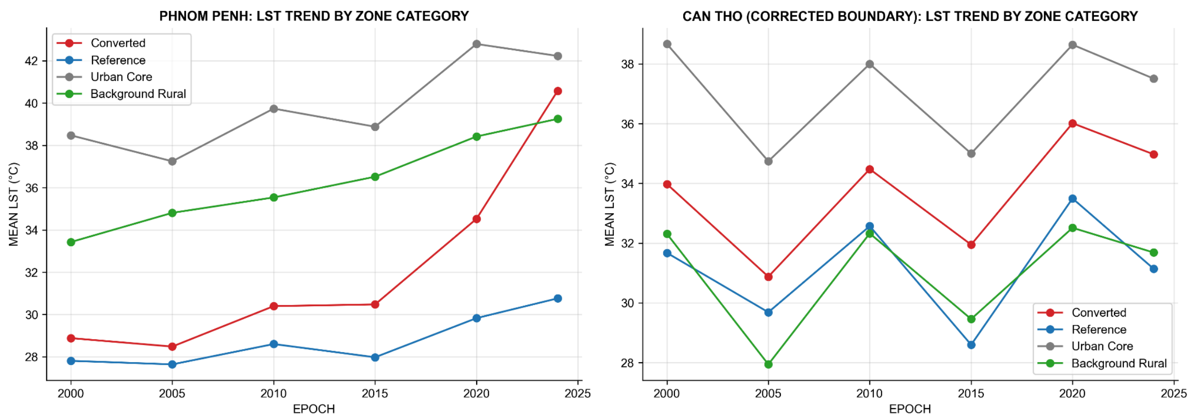

Figure 6. *Mann-Kendall LST trend by zone category, two-panel (Phnom Penh; Can Tho). Corresponds to Table 8, Section 4.1.3, and Table 12, Section 4.2.3.*

5.4 Structural Contrast: Concentrated Versus Diffuse Urbanisation

Section 4.3.2 set out three independent lines of evidence for a structural difference in how the two cities lose cooling infrastructure: cluster dominance, the area-anomaly relationship, and spillover shape. Beyond the finding itself, this contrast has a practical implication. Phnom Penh's pattern, concentrated in a small number of large, identifiable, government-negotiated events, means that a small number of specific site-level interventions (protection or restoration of particular remaining water bodies) could plausibly have an outsized effect on the city's aggregate cooling-loss trajectory. Can Tho's pattern, diffuse across thousands of small, independent conversions with no dominant cluster, does not offer an equivalent small set of intervention points; mitigation would need to operate at the level of peri-urban land-use policy generally rather than through protection of specific named sites, since there are, on this evidence, no equivalent named sites carrying a disproportionate share of the signal.

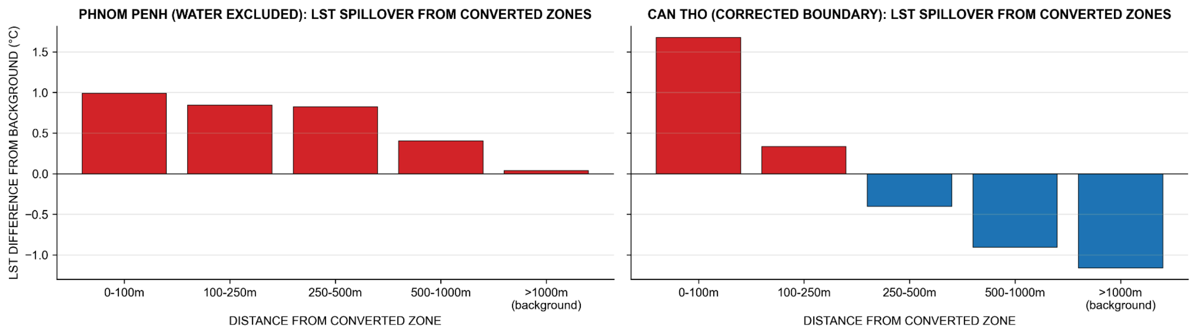

Figure 7. *Mean LST anomaly by distance ring from converted-zone edge, two-panel (Phnom Penh; Can Tho), final epoch. Corresponds to Section 4.1.4 (water-excluded, reported in prose) and Table 13, Section 4.2.4.*

5.5 Seasonal Modulation Revisited

Section 4.3.3 reported a complete sign flip between the two cities (Phnom Penh warmer in the dry season across all four categories; Can Tho warmer in the wet season across all four) and set out the reasoning by which two candidate explanations, LULC misclassification and wet-season scene-timing skew, were tested and ruled out, leaving a genuine regional climatic or geographic difference as the most likely explanation.

This account, however, cannot be the whole story: the sign flip holds not only for the paddy reference category but across all four Can Tho zone categories, including urban core (−3.45°C) and background rural (−1.72°C), neither of which follows an agricultural cropping calendar. A uniform effect across impervious and agricultural land alike points toward a shared atmospheric mechanism rather than a land-cover-specific one. Section 3.8 already notes that cloud-free wet-season composites systematically oversample the clearest, most intensely sunny days between rain events, which can run hotter than typical wet-season conditions; this selection effect, rather than the cropping calendar specifically, is the more likely driver of the sign flip itself, with the paddy-calendar point (Section 4.2.5) better read as describing why the reference category's signal is additionally noisy, not as the primary explanation for the flip. This also sharpens, rather than contradicts, the regional-geography explanation above: Can Tho's flat, low-elevation, humid delta setting is plausibly more susceptible to intense clear-sky heat-trapping between rain events than Phnom Penh's basin setting, making the clear-sky selection effect a specific candidate pathway for the broader geographic difference already proposed, rather than a competing account of it.

Read at the level of what this means for each resource's practical cooling value, the two cities' seasonal patterns point in different directions. Phnom Penh's surviving water bodies, and the wider landscape around them, show comparatively little wet-season cooling relative to the dry season, consistent with open water's high thermal inertia leaving less capacity to cool further once the wet season arrives (Section 4.1.5); this means water bodies retain a meaningful share of their cooling value specifically in the dry season, when heat stress is already highest and the value of cooling infrastructure is greatest. Can Tho's paddy reference category, by contrast, runs warmer in the dry season than the wet season, and its wet-season state is itself a mixture of flooded, transitional and dry-harvested parcels rather than a single, consistent land cover (Section 4.2.5), so paddy's cooling benefit is seasonally and agriculturally contingent in a way that cooling benefit from open water is not.

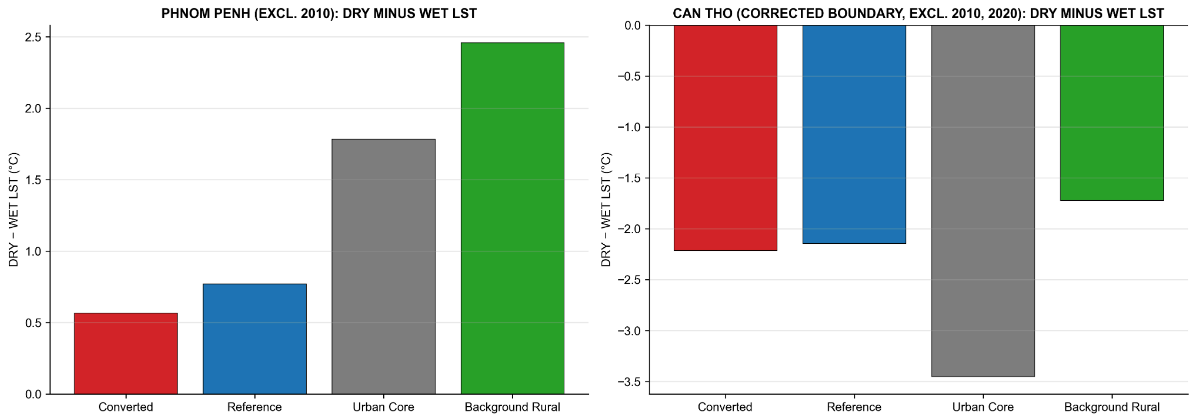

Figure 8. *Dry-season minus wet-season LST differential by zone category, two-panel (Phnom Penh; Can Tho), low-confidence epochs excluded. Corresponds to Table 9, Section 4.1.5, and Table 14, Section 4.2.5.*

5.6 Settlement Morphology and the Proximity-to-Heat Mechanism

Section 4.3.4 found that in both cities, the pre-conversion baseline LST already varies by settlement-morphology class in the same direction as the DiD anomaly, and that for Can Tho, where the comparison could be stated numerically, the baseline gap (2.04°C) exceeds the anomaly gap (1.07°C) between the same two classes. This corroborates, rather than independently explains, the proximity-to-heat mechanism already measured directly by the buffer-spillover analysis (Section 5.4): settlement morphology behaves as a coarse, categorical, one-kilometre-resolution proxy for the same underlying mechanism that the continuous buffer-distance measure captures more precisely. This has a practical corollary: settlement-morphology products such as GHS-SMOD are freely available globally at consistent resolution, whereas a bespoke buffer-distance analysis of the kind used here requires a classified change-detection product as an input. In data-scarce contexts where the latter is not available, settlement-morphology class could serve as a usable, if coarser, proxy for conversion-impact risk. Boeung Kak's status as a named exception to Phnom Penh's own aggregate pattern (Section 4.1.6) is a caution on this corollary: a single, complete, large-scale event overwhelmed the typical buffering that the aggregate settlement-morphology pattern otherwise describes, so a settlement-morphology-based risk screen would have systematically underrated Boeung Kak's eventual impact.

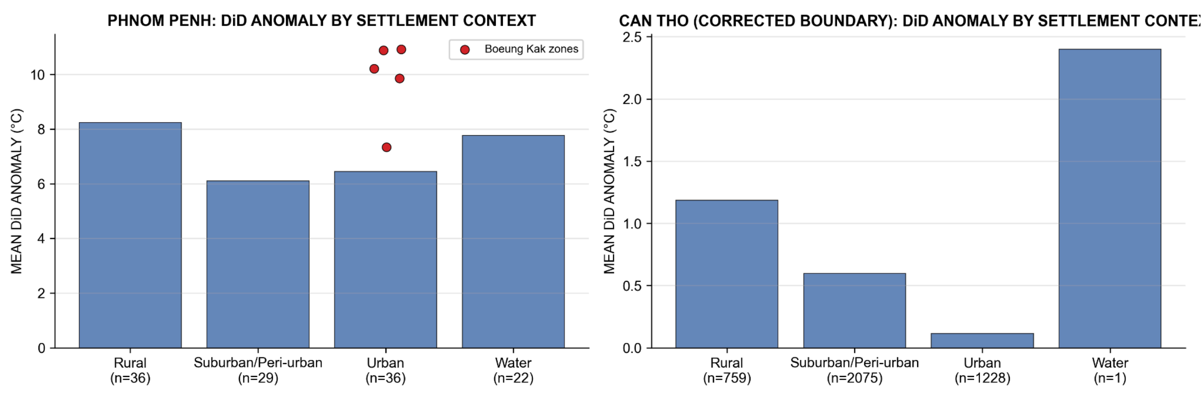

Figure 9. *DiD anomaly by settlement-morphology class, two-panel (Phnom Penh, with Boeung Kak overlay; Can Tho), direct 2000–2024, Unclassified zones excluded. Corresponds to Table 10, Section 4.1.6, and Table 15, Section 4.2.6.*

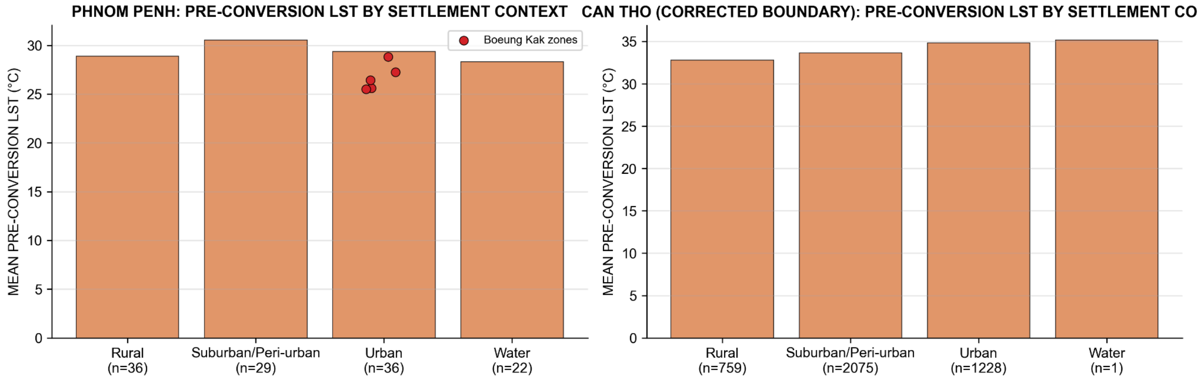

Figure 10. *Pre-conversion baseline LST by settlement-morphology class, two-panel (Phnom Penh; Can Tho), same exclusions as Figure 9. Can Tho values correspond to Table 15, Section 4.2.6; Phnom Penh's equivalent baseline was assessed qualitatively (Section 4.1.6) and is not separately tabulated.*

5.7 Limitations

Several limitations, some already noted at the point they arose in Sections 3 and 4, are drawn together here. Data quality in the surface-reflectance composites underlying the LULC classifications was uneven across epochs and cities. Can Tho's blue band shows elevated haze contamination in three epochs (2000, 2015 and 2024); the 2024 instance was not caught by the original automated plausibility filter, a gap in that filter's coverage rather than a newly arising data problem. Phnom Penh's 2000 composite shows a separate instance of apparent atmospheric haze. Can Tho's 2005 composite carries a more severe, distinct issue, substantial residual cloud speckle across roughly the lower two-thirds of the study extent, which required restricting training-point placement to the upper third to half of the raster for that epoch.

The LULC classification workflow surfaced a general methodological lesson, that point-based training accuracy does not guarantee full-raster classification quality (Section 3.2), which motivated the boundary-correction procedure applied throughout. Even with that procedure, Can Tho's built-up classification ratio against GHS-BUILT-S was unstable across correction rounds for at least one epoch before stabilising, and Can Tho's bare-class area shows large swings across epochs that partly reflect a deliberate methodological choice, reduced training-point targets for that class reflecting genuine on-the-ground land scarcity, rather than purely a land-use signal (Section 3.3). None of Can Tho's six LULC epochs were independently blind-validated in the strict sense of a random-sample recheck performed with no target ratio visible; the possibility of some residual anchoring toward a paddy ratio near 1.0 cannot be fully excluded (Section 3.3).

The three principal remote-sensing datasets underlying this study have different end years (Landsat-derived LST through 2024, GlobalRice500 through 2022, JRC Global Surface Water through 2021), requiring nearest-epoch matching wherever they are cross-referenced; this is a source of imprecision at the single- to three-year scale rather than a structural flaw, but is disclosed as a limitation on the precision of any cross-dataset comparison. Phnom Penh's wet-season LST composites rest on substantially thinner scene coverage than Can Tho's throughout the study period, roughly eight scenes per epoch against roughly twenty-four (Section 4.3.3), warranting broader caution about the Phnom Penh seasonal results specifically.

The reference-zone matching design (Section 3.5) controls for elevation, slope, distance to city centre and aspect, but cannot rule out unmeasured confounders correlated with both conversion likelihood and LST. The minimum mapping unit applied to converted zones (five pixels, 4,500 m²) excludes smaller conversions below that threshold from the matched-zone analyses, though not from the change-detection totals reported in Section 4.

The Mann-Kendall trend analysis (Sections 4.1.3, 4.2.3) is based on only six anchor epochs per series in each city. Six points is a small sample for a non-parametric trend test, limiting statistical power to detect a real trend where one exists, and should be read as a general caveat on both cities' trend results, not only on Can Tho's non-significant findings specifically.

Finally, this study's own experience with the Can Tho administrative boundary (Section 2.1.2) is itself a limitation worth naming explicitly: an incorrect provenance label on a boundary file propagated undetected through several phases of analysis before being caught. Phnom Penh's administrative boundary was found to share the same provenance issue, a citation-only mislabelling rather than a geometric error, on the basis that Cambodia has not undergone an administrative merger comparable to Vietnam's (Section 2.1.1); this conclusion rests on the absence of a known Cambodia-equivalent merger event rather than on an independent geometric re-verification of the Phnom Penh boundary of the kind the Can Tho boundary ultimately received, and is disclosed as a residual, lower-probability risk rather than a confirmed non-issue.

5.8 Future Work

Three specific extensions were identified during this study but not carried out, and are noted here as concrete candidates for future work rather than as findings.

First, distance-binning of Can Tho's converted clusters relative to the Bassac River corridor was considered as a finer-grained companion to the settlement-morphology analysis (Section 4.2.6), on the reasoning that proximity to a major river may modulate conversion impact in a way distinct from proximity to existing built-up area. This was not carried out because it requires OSM river-geometry acquisition for Can Tho equivalent to what this study already obtained for Phnom Penh's water bodies (Section 2.3), which was not in scope here.

Second, during the Phnom Penh LULC classification (Section 3.2), the 2024 epoch's land cover was observed to appear more spectrally clear-cut than earlier epochs, a qualitative impression rather than a quantified result. One plausible interpretation is that wetland ecotone removal, the loss of the graded, mixed-vegetation transition zones that typically border natural water bodies, produces harder, more abrupt land-cover boundaries once those transition zones are gone, in contrast to the more gradual spectral transitions such ecotones would otherwise present. Edge density or mixed-pixel proportion per epoch would be a natural supplementary metric to evaluate this directly; neither was computed in the present study.

Third, none of Can Tho's six LULC epochs received a strict blind validation of the paddy class, in the sense of an independently random-sampled recheck performed with no target validation ratio visible to the reviewer (Section 3.3, Section 5.7). The partial exception is the 2005 and 2010 epochs, whose paddy training points were spatially cross-checked against the GlobalRice500 extent, but this is not equivalent to a full blind revalidation across all six epochs. Such a validation, ideally performed by a second reviewer or after a time delay sufficient to reduce anchoring, would directly test whether the paddy classification's convergence toward GlobalRice500 ratios near 1.0 (Section 3.3) reflects genuine accuracy or residual anchoring, and is recommended before this study's Can Tho paddy figures are treated as fully independent of the validation target used during classification.

6. Conclusion

This study set out to quantify, and directly compare, the land surface temperature consequence of two distinct categories of natural cooling infrastructure loss in rapidly urbanising Southeast Asian secondary cities: urban wetland elimination in Phnom Penh, Cambodia, and paddy conversion in Can Tho, Vietnam. In Phnom Penh (RQ1), water-body loss produced a DiD-corrected LST anomaly of 7.13°C, exceeding H1's hypothesised range (+2 to +5°C) and driven substantially by a small number of large, documented infilling events, Boeung Kak

(9.7–14.5°C) foremost among them. In Can Tho (RQ2), paddy loss produced a smaller anomaly, 0.55°C, falling short of H2's hypothesised range (+1.5 to +3°C) and diffused across thousands of small conversions rather than concentrated in a few dominant clusters; it is nonetheless between roughly two and two-and-a-half times the global paddy-cooling baseline established by Weng et al. (2026).

The comparative synthesis (RQ3) does not resolve to a single answer, and this is itself the finding. Measured as per-unit-area intensity, Phnom Penh's loss is roughly seven times more severe, supporting H3. Measured as total city-wide impact, Can Tho's much larger converted extent gives it the greater aggregate impact instead. Which is the more policy-relevant answer to which resource carries the higher thermal risk depends on whether the question concerns severity per hectare or scale across a city. Methodologically, this study offers a template built entirely from freely available satellite datasets, applicable to any tropical secondary city losing natural cooling infrastructure to urbanisation. Its own experience correcting a mislabelled administrative boundary that had silently propagated through several phases of analysis (Section 2.1.2) is itself a methodological contribution: a concrete demonstration of why dataset provenance should be verified directly rather than trusted from inherited labels.

Acknowledgements

The author gratefully acknowledges the providers of the freely available datasets used in this study: the Landsat Collection 2 Level-2 archive, provided by the U.S. Geological Survey; the JRC Global Surface Water dataset, provided by the European Commission's Joint Research Centre; the GlobalRice500 dataset, made available by Weng et al. (2026) via Zenodo; the Global Human Settlement Layer GHS-BUILT-S and GHS-SMOD products, provided by the European Commission's Joint Research Centre; the Shuttle Radar Topography Mission digital elevation model, provided by NASA Jet Propulsion Laboratory and the U.S. Geological Survey; the Common Operational Dataset – Administrative Boundaries for Cambodia, provided by the UN Office for the Coordination of Humanitarian Affairs and ITOS; the Database of Global Administrative Areas (GADM v4.1); and OpenStreetMap water body geometry, provided by OpenStreetMap contributors. Processing and extraction of most satellite-derived datasets was performed using Google Earth Engine, provided by Google. The analysis was conducted independently, and the findings, interpretations, and conclusions expressed in this paper are those of the author alone.

Data availability

This study's derived geospatial datasets, tabular outputs, and analysis code are openly available on Zenodo at https://doi.org/10.5281/zenodo.21342720 under a Creative Commons Attribution 4.0 International licence. Raw input datasets are publicly available from their respective providers: the Landsat Collection 2 Level-2 archive (https://earthexplorer.usgs.gov/); the Landsat WRS-2 Path/Row grid (https://www.usgs.gov/landsat-missions/landsat-shapefiles-and-kml-files); the JRC Global Surface Water and Shuttle Radar Topography Mission datasets, both accessed via Google Earth Engine (https://earthengine.google.com/); the GlobalRice500 dataset (https://doi.org/10.5281/zenodo.17460919); the Global Human Settlement Layer GHS-BUILT-S and GHS-SMOD products (https://ghsl.jrc.ec.europa.eu/); the Cambodia Common Operational Dataset – Administrative Boundaries (https://data.humdata.org/dataset/cod-ab-khm); the Database of Global Administrative Areas, version 4.1 (https://gadm.org/); the Natural Earth Admin 0 – Countries dataset (https://www.naturalearthdata.com/downloads/50m-cultural-vectors/); and OpenStreetMap water body geometry (https://www.openstreetmap.org/). Empirical analysis, spatial extraction, and visualisation were conducted in Python and its libraries, Google Earth Engine, and QGIS, as described in Section 3.11, Tools and Software.

Declaration of Competing Interest

The author declares that there are no conflicts of interest with respect to the research, authorship, or publication of this article. No financial or personal relationships with any organisation or individual have influenced the work reported herein. This research received no external funding.

Ethics Statement

This research did not involve human participants, animal subjects or any form of clinical intervention. All datasets used are publicly available secondary remote-sensing and geospatial products. Ethical approval was not required and is not applicable for this study.

References

Cai, Z., Guldmann, J.-M., Tang, Y., Han, G., 2022. Does city-water layout matter? Comparing the cooling effects of waterbodies across 34 Chinese megacities. Journal of Environmental Management 324, 116263. https://doi.org/10.1016/j.jenvman.2022.116263.

Farr, T.G., Rosen, P.A., Caro, E., Crippen, R., Duren, R., Hensley, S., Kobrick, M., Paller, M., Rodriguez, E., Roth, L., Seal, D., Shaffer, S., Shimada, J., Umland, J., Werner, M., Oskin, M., Burbank, D., Alsdorf, D., 2007. The Shuttle Radar Topography Mission. Reviews of Geophysics 45, RG2004. https://doi.org/10.1029/2005RG000183.

GADM, 2022. Database of Global Administrative Areas, version 4.1. Available at: https://gadm.org.

Gorelick, N., Hancher, M., Dixon, M., Ilyushchenko, S., Thau, D., Moore, R., 2017. Google Earth Engine: Planetary-scale geospatial analysis for everyone. Remote Sensing of Environment 202, 18–27.

Natural Earth, 2022. Admin 0 – Countries, version 5.1.1, 1:50m Cultural Vectors. Available at: https://www.naturalearthdata.com/downloads/50m-cultural-vectors/.

OCHA/ITOS, 2018. Cambodia – Subnational Administrative Boundaries (COD-AB), admin2, version V_01, valid_on 4 October 2018. Humanitarian Data Exchange. Available at: https://data.humdata.org/dataset/cod-ab-khm.

OpenStreetMap contributors, 2026. Planet dump. OpenStreetMap Foundation. Available at: https://www.openstreetmap.org. Two separate extracts were used: Phnom Penh water bodies, accessed 29 June 2026, and Can Tho water bodies including the Bassac River corridor, accessed 12 July 2026 (both dates determined from local file creation timestamps of the original acquisitions; see Section 2.3).

Pekel, J.-F., Cottam, A., Gorelick, N., Belward, A.S., 2016. High-resolution mapping of global surface water and its long-term changes. Nature 540, 418–422.

Sahmakum Teang Tnaut (STT), 2019. The Last Lakes (Facts and Figures Series No. 40). Phnom Penh: Sahmakum Teang Tnaut.

Schiavina, M., Melchiorri, M., Pesaresi, M., Politis, P., Freire, S., Maffenini, L., Florio, P., Ehrlich, D., Goch, K., Tommasi, P., Kemper, T., 2023. GHSL Data Package 2023. Publications Office of the European Union, Luxembourg. https://doi.org/10.2760/098587.

U.S. Geological Survey, 2018. Landsat World Reference System 2 (WRS-2) Descending (Daytime) shapefile. Available at: https://www.usgs.gov/landsat-missions/landsat-shapefiles-and-kml-files.

Weng, W., Huang, J., Yue, C., Lyu, Z., Xiao, Y., Li, S., Huang, R., Peng, D., Huang, C., Bigirimana, F., Liu, L., Liu, W., 2026. Widespread land surface cooling from paddy rice cultivation revealed by global satellite mapping. Nature Communications 17, 844. https://doi.org/10.1038/s41467-025-67549-z.

Xie, Q., Ren, L., Yang, C., 2023. Regulation of water bodies to urban thermal environment: evidence from Wuhan, China. Frontiers in Ecology and Evolution 11, 983567. https://doi.org/10.3389/fevo.2023.983567.